Comparison of different methods to determine the eruptive potential of selected Active Regions

F. Zuccarello[1], S.L. Guglielmino[1], P. Romano[2], F.P. Zuccarello[3,4,5]

I. Ermolli[6], F. Giorgi[6]

T. Baranyi[7], M.B. Korsos[7], A. Ludmàny[7]

[1]Dipartimento di Fisica e Astronomia - Sezione Astrofisica, Università di Catania, via S. Sofia 78, 95123 Catania, Italy

[2]INAF -- Osservatorio Astrofisico di Catania, via S. Sofia 78, 95123 Catania, Italy

[3]Centre for mathematical Plasma-Astrophysics, KU Leuven, Celestijnenlaan 200B, 3001 Leuven, Belgium.

[4]Royal Observatory of Belgium, Ringlaan 3, 1180 Brussels, Belgium

[5]LESIA, Observatoire de Paris, CNRS, UPMC, Université Paris Diderot, 5 place Jules Janssen, 92190 Meudon, France

[6] INAF- Osservatorio Astronomico di Roma, Via Frascati 33, Monte Porzio Catone, Rome, Italy

[7] Heliophysical Observatory, Research Centre for Astronomy and Earth Sciences, Hungarian Academy of Science, Hungary

Abstract

• Aim of this research is to find observational evidences of signatures and precursors of flares of class M and X occurring in solar active regions.

• We compare the results obtained using three different methods.

• The first method studies the magnetic flux evolution and the magnetic helicity accumulation during a selected time interval relevant to the flare occurrence.

•The second method takes into account the fractal and multi-fractal properties of active regions and how these properties are related to flare occurrence.

• The third approach uses sunspot data derived from the SSD (SOHO/MDI-Debrecen Data) sunspot catalogue.

• The analysis has been carried out on five active regions (NOAA 11166, 11283, 11429, 11515 and 11520).

Magnetic flux and magnetic helicity accumulation

• Using HMI LOS magnetograms, we measured the temporal evolution of the positive, negative, and unsigned magnetic fluxes for the selected ARs.

• To compute the magnetic helicity flux through the photosphere, we determined the mean magnetogram corresponding to the average between two consecutive magnetograms and we measured the horizontal velocity fields by means of the Differential Afine Velocity Estimator technique (DAVE; Schuck 2005, 2006), using a full width at half maximum (FWHM) of the apodizing window of 11 pixels (5”,5) (Schuck 2008). The magnetic helicity flux and the corresponding accumulation of magnetic helicity H for the selected ARs was estimated using the method described by Pariat et al. (2005).

• In each plot the time of occurrence of M-class flares (red vertical lines) and X-class flares (green vertical lines) are reported. When the flare is associated to a CME, the thickness of the vertical line is enhanced.

Magnetic flux: results

AR 166: the plot indicates an increasing trend of the magnetic flux during the selected time interval. The + and – magnetic flux are quite balanced (initially + is slightly higher, but after 80 hours the situation is reversed).

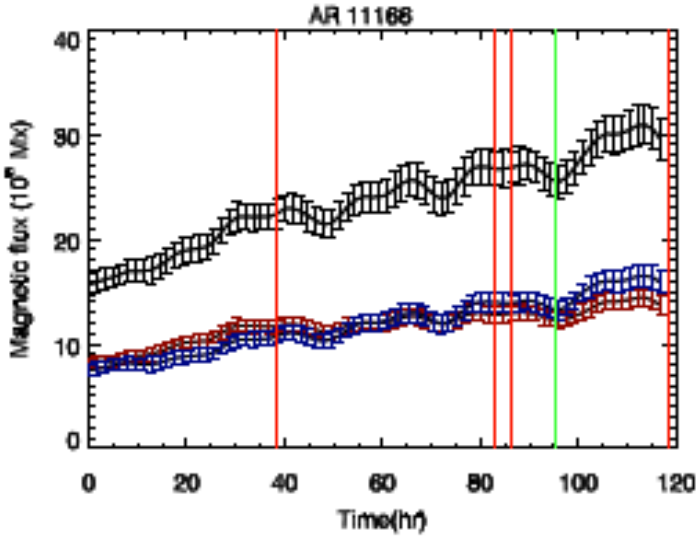

AR 283: the – magnetic flux is almost constant, while + decreases during the selected time interval. The positive and negative magnetic fluxes show an imbalance, with a higher - flux, increasing in time.

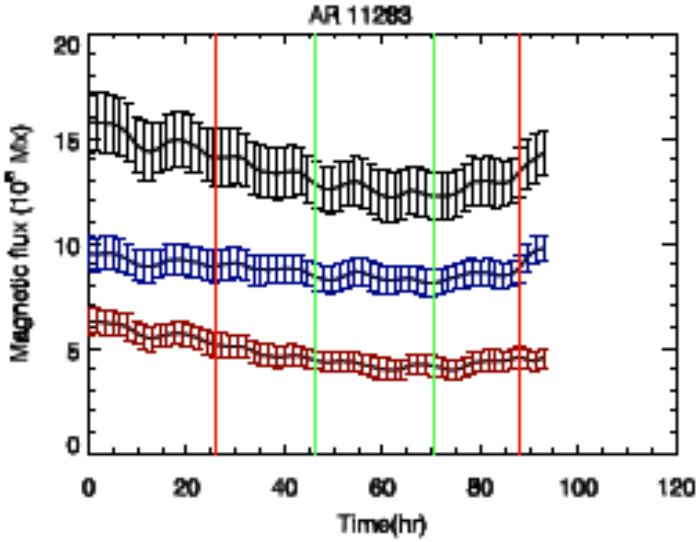

Magnetic flux: results

AR 429: the **– flux decreases** during the selected time interval, while the **+** is **almost constant**. At the beginning there is a **flux imbalance** such that the – flux is about 1.66 times +, but **later** on the imbalance **decreases**.

AR 515: the **- flux** is **almost constant**, while **+ increases continuously**. **Initially - > +**, but **after** t =70 hours **the situation is reversed**. Interestingly, this **time coincides with an M-class flare associated to a CME** and with a change in the slope of the magnetic helicity (see next plots).

AR 520: the **- flux decreases** continuously, while **+ is almost constant**. Initially - > +, but at time t = 65 hours, the situation is reversed. Also in this case the **time of reversal corresponds to a flare** (X-class) associated to a **CME** and to a (greater) change in the slope of the accumulated magnetic helicity.

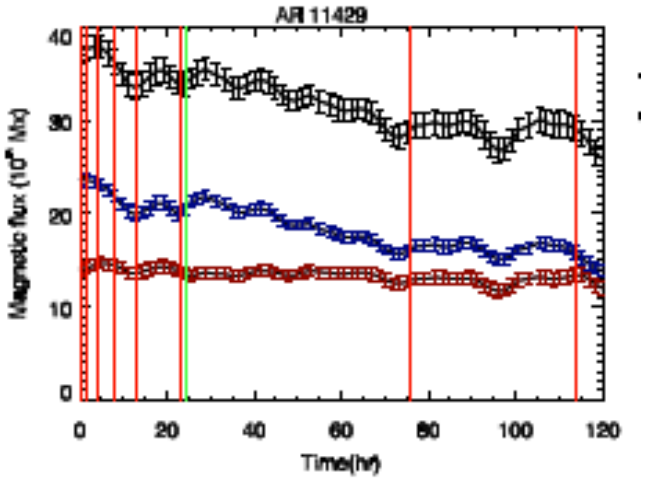

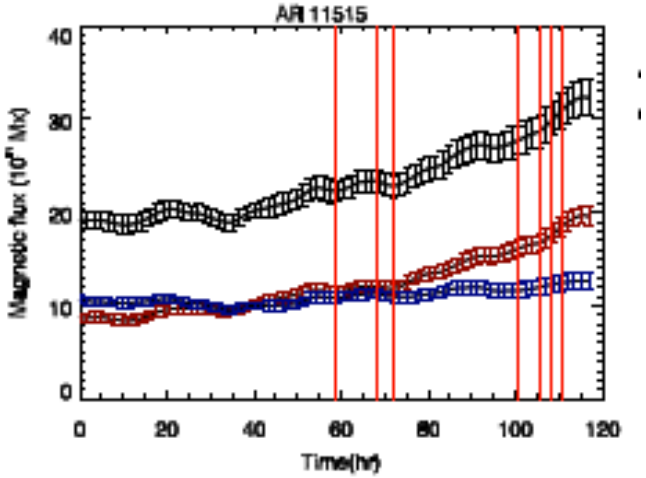

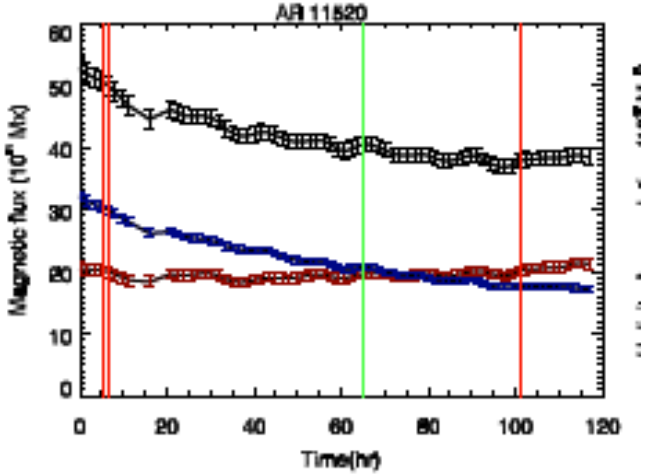

Magnetic helicity accumulation: results

AR 166: **H is positive** and shows a **continuous increase** during all the selected time interval; **no change in H after** the M-class **flare** associated to a CME and similarly after the X-class flare.
To be noted a flattening of the H trend after the second M-class flare, followed by a new increase after the occurrence of the third M-class flare.
This AR did not follow the hemispheric helicity rule.

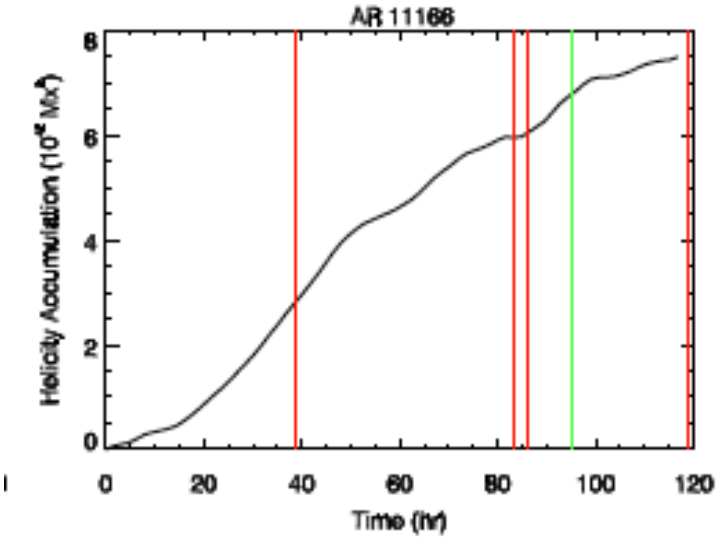

AR 283: the **H** general trend **is positive and increases continuously** until the last **M-class flare** (associated to a CME) takes place, when it shows a **rapid decrease**.
The values of H are almost one order of magnitude lower than for AR 166.
The AR does not follow the hemispheric helicity rule.

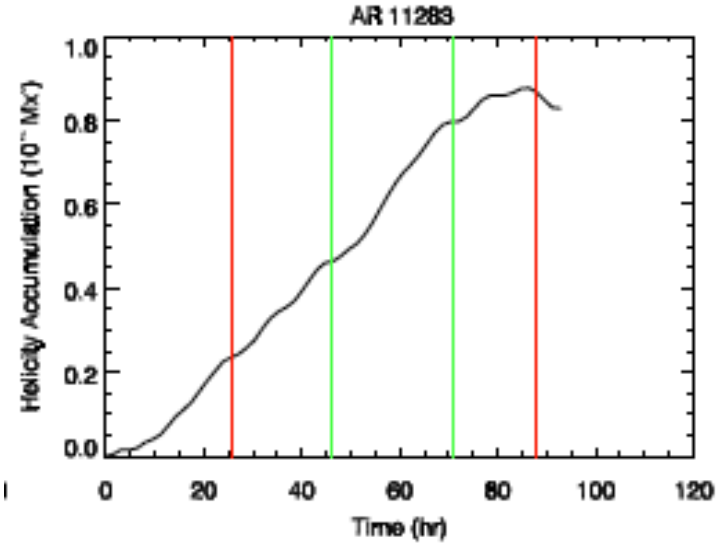

Magnetic helicity accumulation: results

AR 429: very rapid **increase of the negative** magnetic helicity **until an X-class flare**, associated to a CME, occurs. Later, for almost 50 hours, H remains approximately constant and, **after the occurrence of an M-class flare associated to a CME, a new**, smoother **increase of H** accumulation takes place. This AR did not follow the Hale Law, but it followed the helicity hemispheric rule.

AR 515: initially, for 12 hours, H remains close to zero (during the same Δt the magnetic flux remains constant). Later, H starts to increase (**negative**) and shows a phase of flattening after the second M-class flare associated to a CME; later on it **increases** again, **without any clear signature of variation after** some M-class **flares**.

AR 520: **H increases very rapidly** during the first 10 hours, and **later the increase is smoother**, until when a maximum is reached. Then an **X-class flare**, associated to a **CME**, takes place. After this event **H starts to decrease.**

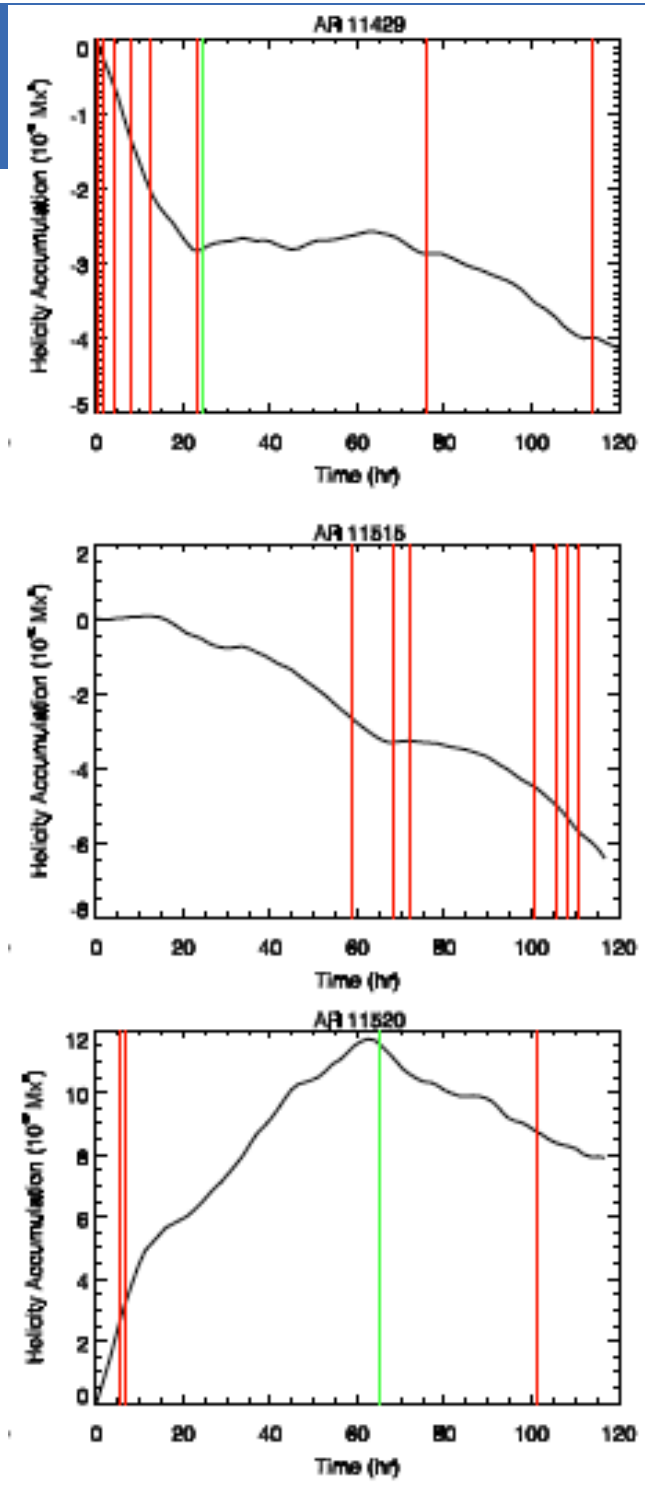

Magnetic flux and magnetic helicity accumulation: results

Parameter	AR 166	AR 283	AR 429	AR 515	AR 520
AR classification	$\beta\gamma\delta$	$\beta\gamma\delta$	$\beta\gamma\delta$	$\beta\gamma\delta$	$\beta\gamma\delta$
CM passage	Mar 8, 2011	Sept 5, 2011	Mar 8, 2012	Jul 2, 2012	Jul 12, 2012
Average Lat	N11	N13	N17	S17	S17
Hale Law	Yes	Yes	No	Yes	Yes
Φ_{max} (Mx)	3.1×10^{22}	1.6×10^{22}	3.9×10^{22}	3.2×10^{22}	5.3×10^{22}
Φ imbalance	$\Phi_+ \sim 1.1 \times \Phi_-$	$\Phi_- \sim 2 \times \Phi_+$	$\Phi_- \sim 1.6 \times \Phi_+$	$\Phi_+ \sim 1.5 \times \Phi_-$	$\Phi_- \sim 1.5 \times \Phi_+$
H max (Mx^2)	8.0×10^{42}	8.5×10^{41}	-4.1×10^{42}	-6.4×10^{42}	1.2×10^{43}
H Sign	Positive	Positive	Negative	Negative	Positive
Hemispheric rule	No	No	Yes	No	Yes

- The magnetic flux imbalance and the reversal of sign of the most prominent magnetic flux seems to be often related to flare/CME occurrence
- In some of the ARs analyzed the accumulated magnetic helicity changes its slope after a flare/CME occurrence, but a general rule cannot be claimed at time of the current analysis.

Fractal and multi-fractal properties of ARs

Several studies indicate distinct values of the fractal and multifractal parameters measured on ARs that have hosted flares of different class.

However, these measurements are considered to be rather inefficient tools for distinguishing ARs on the basis of the flare activity, because of the large dispersion of values measured on ARs that have produced the same class of events.

Nevertheless, the distinct values of the parameters measured on ARs hosting extreme-class flares constitute a tool for outlining the future evolution of a region just appeared on the solar disk, by narrowing the class of flares it may host before the occurrence of any events.

Fractal and multi-fractal properties of ARs

- The fractal and multifractal parameters of the selected ARs were measured on the time series of SDO/HMI Level 1.5 LOS full-disc magnetograms

- The longitudinal distance of the selected ARs was within ±30◦ of the central meridian.

- The whole data set consists of 2402 magnetograms, each of 4096 x 4096 pixels, with a pixel size of 0.505 arcsec and cadence of 720 s.

- We computed the generalized fractal dimension D_0 and D_8, and the multifractal Contribution Diversity C_{div} and Dimensional Diversity D_{div} on each image of the analyzed series.

- The flaring level is described by the flare index (FI), computed assuming the flare history of the region depicted by the NOAA's GOES X-ray archive, and by considering the most intense event hosted by the region (Max FI).

Fractal and multi-fractal properties of ARs : results

Results derived from unsigned flux data of the analyzed ARs.

Analysis of the series confirms previous findings by Giorgi et al. (2014) on the different evolution of the fractal and multifractal parameters derived from each analyzed AR.

They also confirm the different evolution of the same parameters when taking into account trailing and leading flux data in the analyzed region.

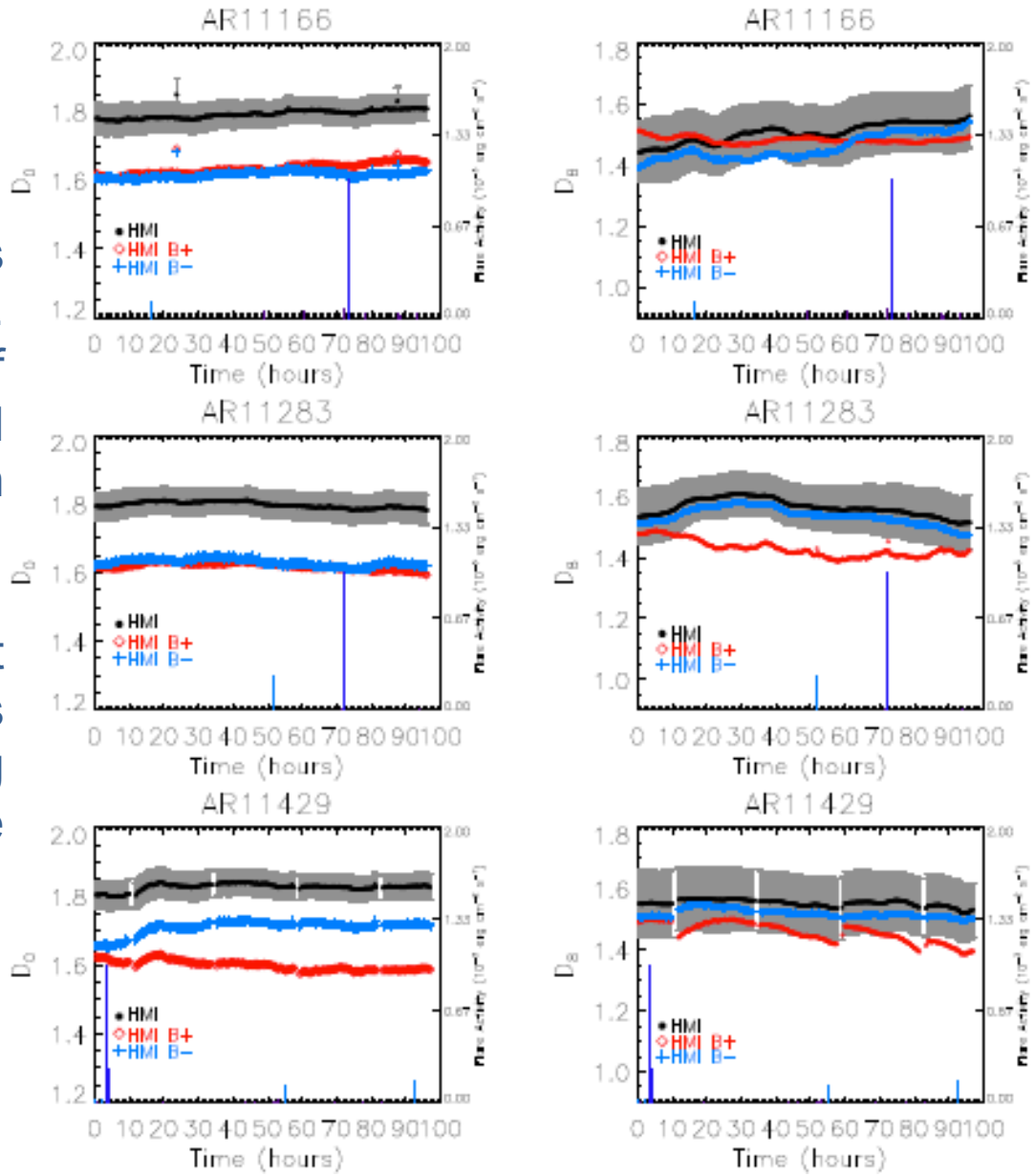

Fractal and multi-fractal properties of ARs : results

The results obtained show a systematic larger variance of the values derived from trailing flux data in the analyzed AR than obtained from both unsigned and leading flux data.

However, the variance of values derived from each AR lacks distinctive signatures of the flaring level of the analyzed region, as already reported in the literature.

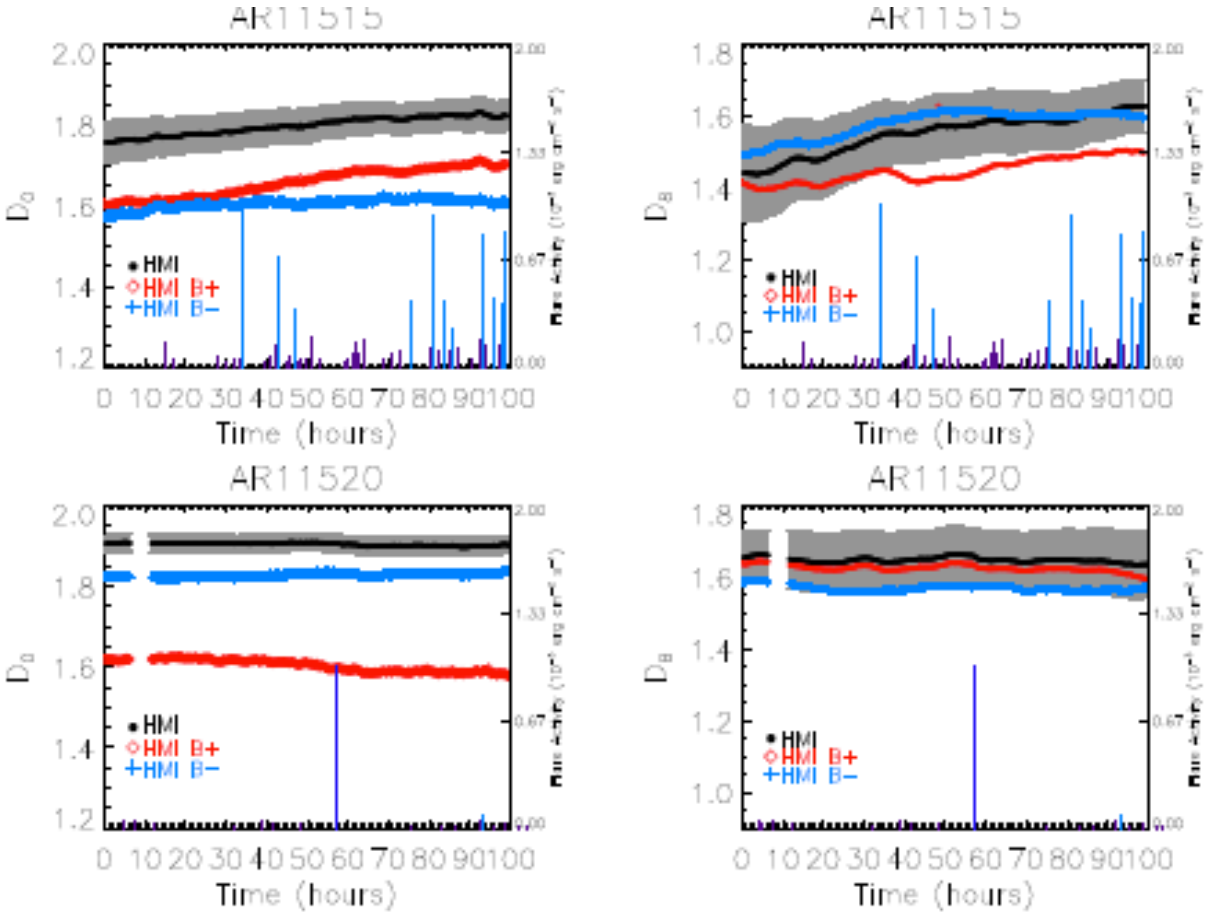

Fractal and multi-fractal properties of ARs : results

Several flares occur during a decreasing phase of the D_{div} and an increasing phase of the D_8 values estimated by considering unsigned and signed flux data of the leading polarity of the AR hemisphere.

However, these features of the parameter trends were not found to be a consistent pre-flare signature in the whole AR sample and events, confirming previous results in the literature.

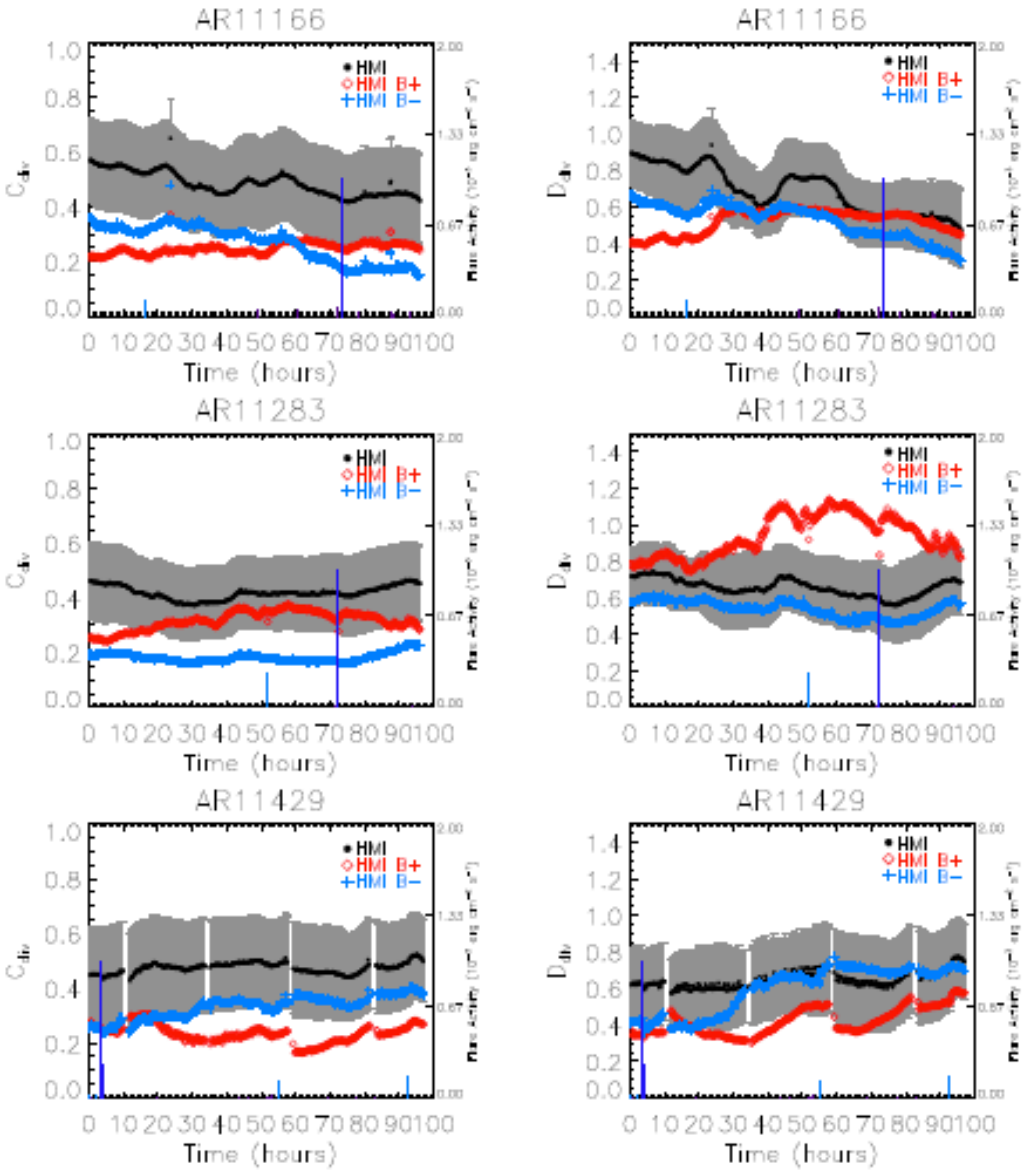

Fractal and multi-fractal properties of ARs : results

Relation between the average value of the parameters estimated for each AR and its FI and Max FI, respectively.

Slightly higher values of fractal D_8 parameters, as well as a lower value of C_{div}, imply a higher flare activity of the ARs, in terms of its FI that accounts for the flare size and event frequency (see, e.g. Giorgi et al. 2014).

However, the signature of the AR flaring activity in the analyzed parameters is feeble, and this holds also when the measured values are considered with respect to the Max FI.

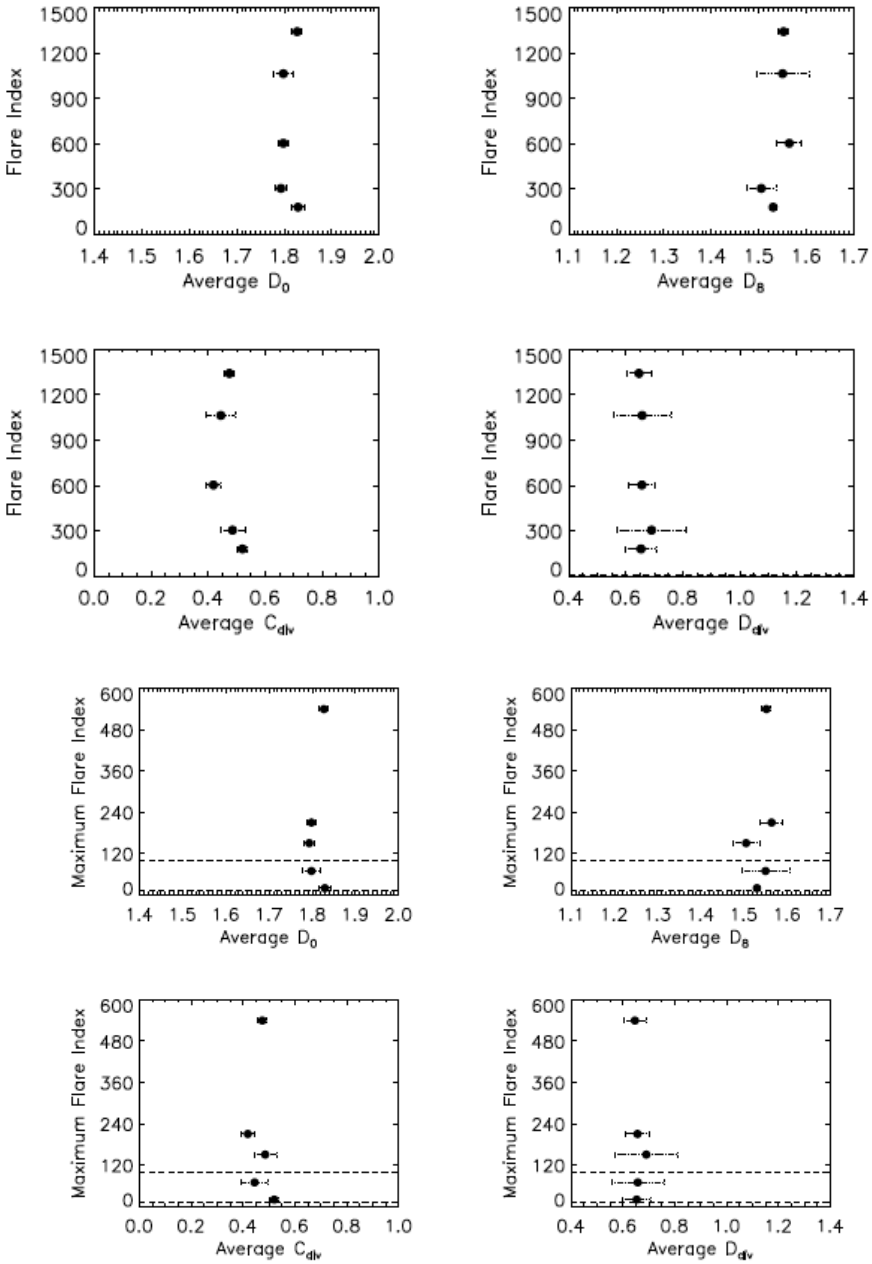

Fractal and multi-fractal properties of ARs : results

Table 1. Summary of the average value and standard deviation of the fractal (D_0 and D_8) and multifractal ($C_{\rm div}$ and $D_{\rm div}$) parameters measured in our sample of five ARs, by considering unsigned flux data in the analyzed ARs.

AR	166	283	429	515	520
D_0	1.79 ± 0.02	1.79 ± 0.01	1.82 ± 0.01	1.80 ± 0.02	1.904 ± 0.003
D_8	1.50 ± 0.03	1.56 ± 0.03	1.55 ± 0.01	1.55 ± 0.05	1.647 ± 0.008
$C_{\rm div}$	0.48 ± 0.04	0.42 ± 0.02	0.47 ± 0.02	0.44 ± 0.05	0.46 ± 0.01
$D_{\rm div}$	0.69 ± 0.12	0.66 ± 0.05	0.65 ± 0.04	0.66 ± 0.10	0.57 ± 0.02
FI	303.6	602.7	1342.6	1064.1	444.3
Max FI	150	210	540	69	140

In agreement with previous findings reported in the literature, these derived values do not allow us distinguishing the X- and M-class flaring ARs of the analyzed sample.

Pre-flare dynamics of sunspot-groups

In previous studies it was found that a good indicator of the flaring activity is the inter-spot gradient of the magnetic flux (Korsòs et al. 2014):

$$G_M = \left| \frac{f(A_1) \cdot A_1 - f(A_2) \cdot A_2}{d} \right|$$

A denotes the spot area, *d* is the distance between the two spots and *f (A)* is the mean magnetic flux density expressed as a function of spot area: $B_{mean} = f(A) = 265 \cdot \ln(A) + 1067$ [gauss].

The product *f(A) ·A* is the measure of flux amount in the spot umbra.

Previous studies indicate that the pre-flare variation of G_M starts with a more or less steep rise until a maximum, followed by a decrease, is reached until the flare onset.

It was an important common property that the eruption was preceded by the G_M decrease in all the cases analyzed.

Pre-flare dynamics of sunspot-groups

In this study we take into account all spots of a small subgroup at the inversion line.

A small area is selected in each case, which contains spots of opposite polarities very close to each other.

- the flux amounts have been computed for all involved spots

- the distance *d* has been computed between the centroids of the subgroups of opposite polarities.

Pre-flare dynamics of sunspot-groups: results

AR NOAA 11520

Left column:

-variation of G_M,

- variation of the total flux of the selected subgroup

-variation of the distance of the centers of weigth of the subgroups of opposite polarities.

Right column:

- white-light image of the active region,

-reconstruction of the active region from the HMIDD catalogue, indicating the small selected subgroup to be followed

- magnetogram of the active region.

LCM: longitudinal distance from the central meridian

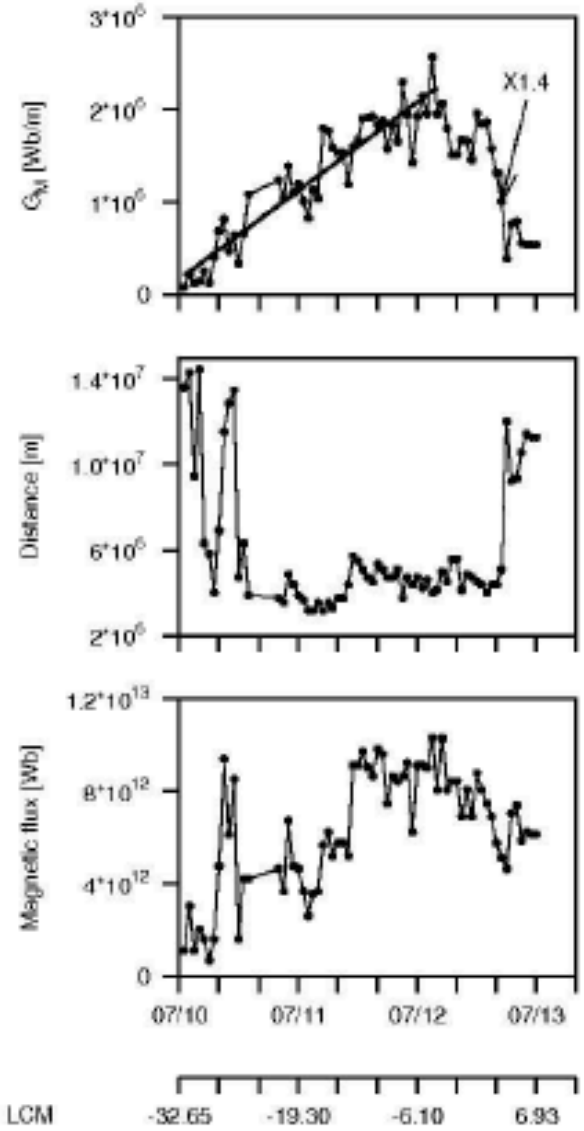

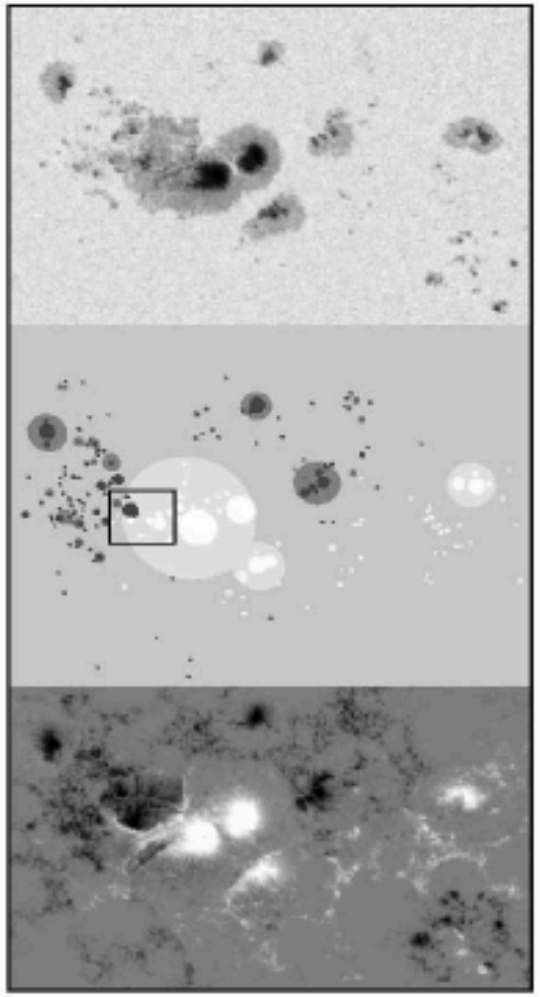

Pre-flare dynamics of sunspot-groups: results

The X1.5 flare of AR NOAA 11166 is preceded by the mentioned behaviour of G_M, the flare occurs on the decaying phase after the maximum.

In AR NOAA 11283 two X-class and two M-class flares have been observed.

The pre-flare patterns are recognizable, but the applicability of the method may be restricted because several flares are fed by the accumulated free energy

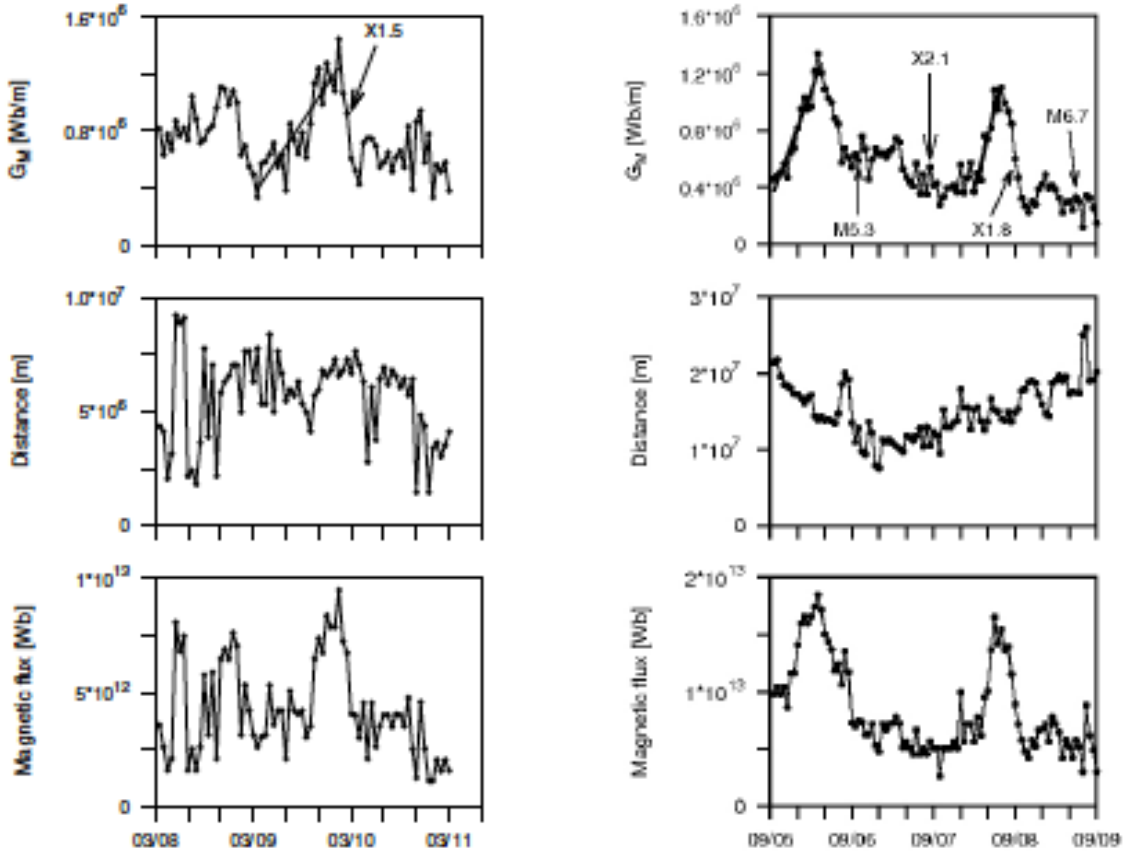

Diagrams of ARs NOAA 11166 and 11283

Pre-flare dynamics of sunspot-groups: results

Another diagnostic tool is the relationship between the values of the maxima and the S intensities of the flares after them:

$$S_{flare} = a \cdot G_{Mmax} + b$$

where $a = 2.7 \cdot 10^{-11} \pm 0.4 \cdot 10^{-11}$ (watts/m^2)/(Wb/m)
and $b = 3.4 \cdot 10^{-5} \pm 0.7 \cdot 10^{-5}$ watts/m^2

This is the equation of a linear regression line obtained on a statistical sample of 57 cases observed using SOHO/MDI data.
This equation describes the relationship between the accumulated free energy, represented by G_M as a proxy measure, and the released energy represented by the GOES-class as another proxy measure.

Pre-flare dynamics of sunspot-groups: results

Table 1. ARs and flares

AR NOAA 11...	Time Y.M.D H:M	G_M max. $\cdot 10^6$Wb/m	Obs.int.	Pred.int.	pred/obs	Δt hours
166	11.03.09 23:23	1.4	X1.5	M7.18	0.48	04
283	11.09.06 01:50	1.3	M5.3	M6.91	1.30	14
	11.09.06 22:20	1.3	X2.1	M6.91	0.33	34
	11.09.07 22:38	1.1	X1.8	M6.37	0.35	03
	11.09.08 15:45	1.1	M6.7	M6.37	0.95	19
429	12.03.07 00:24	4.6	X5.4	X1.58	0.29	12
	12.03.09 03:53	2.2	M6.3	M9.34	1.48	04
	12.07.10 17:44	2.4	M8.4	M9.88	1.18	05
515	12.07.02 10:52	1.5	M5.6	M7.45	1.33	10
	12.07.04 09:55	1.8	M5.3	M8.26	1.56	09
	12.07.04 22:09	1.4	M4.6	M7.18	1.56	03
	12.07.05 03:36	1.4	M4.7	M7.18	1.53	02
	12.07.05 11:44	1.4	M6.1	M7.18	1.18	10
520	12.07.12 16:49	2.5	X1.4	X1.02	0.73	14

Pre-flare dynamics of sunspot-groups: results

- The ratios of predicted/observed intensities show a large scatter, their average is 1.02 so the regression line seems to be a good approximation but the standard deviation of these ratios from the average is 0.49.

- Two thirds of the time differences between G_M maxima and flare onsets are within 10 hours, this was also a predominant time interval in Korsòs et al. (2014).

- The performance of this approach may be improved. Further development is in progress to extend the forecast for the cases of multiple flares by following the free energy vs. released energy budget of the active region.

- The forecast of the onset time can also be precised by examining the possible signatures in the variations of the distance of polarities and the flux amount.

Conclusions

Our results can be summarized as follows:

- The magnetic flux imbalance and the reversal of sign of the most prominent magnetic flux seems to be often related to flare/CME occurrence
- In some of the ARs analyzed the accumulated magnetic helicity changes its slope after a flare/CME occurrence, but a general rule cannot be claimed at time of the current analysis.
- The measured values of fractal and multi fractal parameters do not allow us to discern the ARs depending on their flaring level, if measurement uncertainties are taken into account.
- The pre-flare variation of G_M starts with a more or less steep rise until a maximum, followed by a decrease, is reached. Later the flare onset is observed.
- It is important to extend this forecast method for the cases of multiple flares.

Acknowledgments

This research work has received funding from the European Commissions Seventh Framework Programme under the grant agreements no. 284461 (eHEROES project), no. 312495 (SOLARNET project), no. 606862 (F-Chroma project). This research is also supported by the ITA MIUR-PRIN grant on “The active sun and its effects on space and Earth climate" and by Space WEather Italian COmmunity (SWICO) Research Program.